Two propagation scenarios of isolated breakdown lightning processes in failed negative cloud-to-ground flashes

Ivana Kolmašová
Department of Space Physics, Institute of Atmospheric Physics of the Czech Academy of Sciences, Prague, Czechia
Faculty of Mathematics and Physics, Charles University, Prague, Czechia

Ondřej Santolík
Department of Space Physics, Institute of Atmospheric Physics of the Czech Academy of Sciences, Prague, Czechia
Faculty of Mathematics and Physics, Charles University, Prague, Czechia

Eric Defer
Laboratoire d'Aérologie, Université de Toulouse, CNRS, OMP, UPS, Toulouse, France

Petr Kašpar
Department of Space Physics, Institute of Atmospheric Physics of the Czech Academy of Sciences, Prague, Czechia

Andrea Kolínská
Department of Space Physics, Institute of Atmospheric Physics of the Czech Academy of Sciences, Prague, Czechia
Faculty of Nuclear Sciences and Physical Engineering, Czech Technical University, Prague, Czechia

Stéphane Pedeboy
Météorage, Pau, France

Sylvain Coquillat
Laboratoire d'Aérologie, Université de Toulouse, CNRS, OMP, UPS, Toulouse, France

Corresponding author: I. Kolmašová, Institute of Atmospheric Physics of the Czech Academy of Sciences, Boční II 1401, 141 00 Prague 4, Czechia (iko@ufa.cas.cz)

Key points

- Preliminary breakdown radiowave pulses typical for negative cloud-to-ground flashes are exceptionally observed without return strokes.
- This phenomenon could be explained by the presence of an unusually strong positive charge region in the lower part of the thundercloud.
- Data show evidence of two possible propagation scenarios: the discharge leader either extends horizontally inside the cloud or fades out.

Plain language summary

Visible lightning return stroke represents a well-known manifestation of atmospheric electricity. However, it is only the last stage of a complex sequence of phenomena that starts inside an electrically charged thundercloud by a preliminary breakdown process, continues by a stepped leader that moves electrical charges into the lightning channel, neutralized eventually by a large return stroke current and followed in most cases by processes leading to subsequent strokes. All these phenomena occurring inside or below the thundercloud involve impulsive electrical currents and hence emit radio waves. Analysis of our observations of isolated breakdown radiowave pulses, which are not followed by a return stroke shows that the underlying processes are similar to a usual preliminary breakdown preceding negative cloud-to ground discharges. Nevertheless, a strong positive charge layer at the bottom of the thundercloud can force the breakdown current pulses to keep flowing inside the cloud or die out, and thus prevents them from evolving into a return stroke that would move the negative charge from the cloud to the ground.

Abstract

Isolated breakdown (IBD) process is a lightning phenomenon that was rarely reported in the past. It is characterized by radiowave pulses typical for preliminary breakdown before negative cloud-to-ground flashes, which fail to evolve into return strokes. We identified 128 IBD pulse trains in measurements collected in the Mediterranean by a broadband receiver (0.005 – 37 MHz) in 2015 and 2018. By combining these records with concurrent Lightning Mapping Array measurements of very high frequency radiation (60 – 66 MHz) emitted by in-cloud discharges we investigate the development of each discharge. We identify two scenarios: either the discharges continue to propagate almost horizontally for more than 150 ms (73%), or they disappear sooner, typically within several tens of milliseconds (27%). Using numerical modeling, we verify that a potential barrier inside the thundercloud caused by a strong lower positive charge center could indeed block further propagation of lightning leaders toward the ground.

Index terms: 3304 Atmospheric electricity

3324 Lightning

3394 Instruments and techniques

1. Introduction

Both cloud-to-ground (CG) and intracloud (IC) lightning flashes usually start with a preliminary breakdown (PB) process (sometimes referred to as initial breakdown) which is characterized by a presence of trains of bipolar pulses in electromagnetic recordings (Marshall et al., 2014a and references herein). These pulse trains are emitted by in-cloud currents and can be detected hundreds of kilometers from their source (Kolmasova et al., 2016, Kotovsky et al., 2016). Measurements conducted several kilometers from lightning recently showed that the first PB pulse is preceded by an ionizing initiation event followed by an initial electric field change (Marshall et al., 2014b, 2019). The PB stage of CG lightning flashes usually converts into a stepped leader followed by the first return stroke (RS) (Rakov & Uman, 2003 and references herein).

However, sometimes the pre-stroke activity does not lead to a regular RS pulse. Norinder and Knundsen (1956) reported for the first time an observation of “pre-discharges lacking the main discharge”. Nag and Rakov (2008) described observation of electric field pulses typical for PB process, which were not followed by RS pulses. They named them “first attempted cloud-to-ground leaders” and found that about 18 % of CG discharges with peak currents below 15 kA reported by NLDN were in reality attempted leaders. As the term “attempted leader” is also used for downward moving K-changes (Rakov and Uman, 2003), failed dart leaders (Rhodes et al., 1994) or for failed leaders observed below the cloud base (Tran and Rakov, 2016) we will rather use a term “isolated breakdown (IBD)”. Sharma et al. (2008) compared properties of IBD pulse trains with those leading to subsequent lightning activity. They found that durations of pulse trains and inter-pulse time intervals were comparable for IBD and PB pulse trains. Kolmasova et al. (2018) showed that an intense radiation in a frequency band from 60 to 66 MHz abruptly started with the first pulse and was present during the entire initiation phase of both regular PB or IBD processes.

To our knowledge, a specific model describing the IBD process has not yet been designed. Nevertheless, existing probabilistic models can simulate propagation and branching of lightning channels inside positive and negative charge regions for IC discharges (Mansell et al., 2002; Tan et al., 2006; Riousset et al., 2007). These models usually use electric field threshold to allow propagation of a discharge. In the model by Bazelyan and Raizer (2000) the lightning channel extends until the difference between the potential of the channel tip and the ambient potential is sufficiently high. Tan et al. (2014) found that the types and polarities of lightning discharges might depend on locations and magnitudes of oppositely charged layers near initiation points. For negative CG flashes, the magnitude of the lower positive charge region (LPCR) near the lightning initiation needed to be strong enough for initiation breakdown, however an exceptionally strong LPCR could obstruct further propagation of the discharge down to the ground. Iudin et al. (2017) similarly concluded that a strong LPCR could block further vertical extension of the discharge.

In the present letter, we report results of our investigation of propagation schemes of the IBD processes. Our analysis is based on a combination of broadband magnetic-field measurements, narrowband electric-field Lightning Mapping Array measurements, and numerical modeling of the LPCR. The data were collected in the Mediterranean during two observational campaigns in September - November 2015 and September - November 2018 in the frame of the SOLID (Space-based Optical LIghtning Detection) and the EXAEDRE (EXploiting new Atmospheric Electricity Data for Research and the Environment) projects, respectively. Properties of observed IBD events are similar to these preceding negative CG discharges, which only do not succeed to reach the ground. We present for the first time two typical scenarios of IBD processes: (i) discharge leaders keep propagating horizontally for more than 150 ms (73%) or (ii) they substantially weaken sooner, usually within several tens of milliseconds (27%). Our modeling results support the hypothesis that an unusually strong LPCR inside the thundercloud can be responsible for an occurrence of the IBD phenomenon by blocking the downward propagation of the developing negative CG discharge. In sections 2 and 3 we describe our instrumental setup and our dataset. In section 4, we analyze the measurements. In section 5, we introduce our model and illustrate how the LPCR strength influences propagation of discharges. In section 6, we discuss and summarize our results.

2. Instrumentation

To detect fluctuations of the E-W horizontal component of magnetic field we use a broadband analyzer BLESKA (Broadband Lightning Electromagnetic Signal Keeper Analyzer) (Kolmasova et al., 2018), a clone of the IME-HF analyzer (Instrument de Mesure du champ Electrique Haute Fréquence) developed for the TARANIS (Tool for the Analysis of Radiation from lightning and Sprites) spacecraft (Blanc et al., 2007) and adapted for ground-based measurements. The analyzer is connected to the magnetic sensor SLAVIA (Shielded Loop Antenna with a Versatile Integrated Amplifier) and detects signals in the frequency range from 5 kHz to 37 MHz, sampled at 80 MHz. The absolute time is obtained from a GPS receiver with an accuracy of 1 μs. The duration of triggered waveform snapshots is 208 ms. The receiver was installed close to Ersa, France (550 m, 42.97°N, 9.38°E), at the northernmost point of the Corsica island, in 2015. It was moved by several kilometers in 2018 (100 m, 43.00°N, 9.36°E). BLESKA detects broadband pulses exhibiting peak-to-peak amplitudes larger than 0.4 nT which is well above the level of environmental interferences.

The magnetic field data are combined with the measurements of 12-LMA-station SAETTA (Suivi de l'Activité Electrique Tridimensionnelle Totale de l'Atmosphère) network operated in Corsica since June 2014 (Coquillat et al., 2019). Each station is equipped with an electric-field antenna and detects very high frequency (VHF) radiation emitted by cloud discharges in the 6 MHz bandwidth centered at 63 MHz, sampled at 25 MHz. In each 80-µs time interval, the individual stations identify the times of arrival of the strongest VHF peak exceeding a predefined threshold. The arrival times of the radiation peaks coming from the same source and detected by at least six individual LMA stations are used to calculate the 3D-location of a VHF radiation source. SAETTA also estimates power of individual geo-located VHF sources. GPS receivers are connected to each LMA station and provide an accurate time assignment.

Locations, polarities, and peak currents for discharges included in our study were provided by the French lightning locating system Météorage. To achieve an optimum coverage of the South-East France and Corsica regions it combines sensors installed across France, and sensors operated by Italian national service SIRF. The detection efficiency is 94%, the median location accuracy 120 meters (Pedeboy and Toullec, 2016) and the accuracy of estimation of peak current amplitudes is about 18% (Schulz et al., 2016). Characteristics of both CG and IC discharges were available for both 2015 and 2018 datasets with an improved detection efficiency for the 2018 IC discharges.

3. Dataset

We visually inspected all triggered 208-ms long magnetic-field waveform captures recorded by BLESKA during autumn 2015 and autumn 2018 in order to identify sequences of bipolar pulses. To distinguish IBD events from usual PB pulses preceding negative CG lightning we used the following criteria:

i) RS pulses were absent after the initial pulse sequence within the 208-ms long magnetic-field waveform snapshots.

ii) The list of Météorage detections did not contain any CG detection within 1s after the time of the strongest IBD pulse in magnetic field records.

iii) Knowing that the usual PB pulses have the same initial polarity as the corresponding RS pulses (Rakov and Uman, 2003) we selected only trains of pulses that exhibited the same polarity as negative RS pulses. This criterion together with the visual inspection of the pulse shapes leads to the exclusion of PB pulses preceding the IC discharges. We were able to check the pulse polarity without any ambiguity by combining the magnetic loop antenna orientation with locations of pulses detected by Météorage.

As following step, we have chosen only the magnetic-field records containing IBD pulse trains during which SAETTA was able to geo-locate at least one VHF source. Raw data from individual SAETTA stations were also investigated. The resulting dataset consists of 128 IBD events (33 events in 2015; 95 events in 2018).

4. Data Analysis

The sequences of IBD pulses identified in the magnetic-field records were usually several milliseconds long. They were preceded by an electromagnetically quiet period lasting several tens of milliseconds in all cases. The inter-pulse intervals lasted several tens of microseconds. The strongest pulses in individual sequences usually occur during the first millisecond after the first recognizable pulse. The pulse activity following the sequences of IBD pulses was weak or completely absent. The sequences of pulses therefore did not differ from trains of PB pulses preceding negative CG discharges (e.g., Kolmasova et al., 2014, 2018, 2019, Smith et al, 2018, and Nag et al, 2009). Two examples of magnetic-field waveforms containing IBD events recorded by BLESKA are shown in Figs. 1a and 2a, displaying a detail of 3 ms, while Figs. panels 1b, 1c, 2b, and 2c present the whole 208-ms long waveforms. Waveforms in Fig. 1 and Fig. 2 were respectively captured on October 2, 2018 and October 13, 2015. Red arrows point at the time of IC discharges detected by Météorage. Their peak currents were estimated to 16.2 kA and 9.4 kA, respectively.

Correspondence of magnetic-field IBD pulses measured by BLESKA and sources of VHF radiation geo-located by SAETTA is shown in Fig.1a, 1b, 2a, and 2b: each dot corresponds to one reconstructed source of VHF radiation color-coded by its power. It is evident from Figs. 1a and 2a that almost none of the observed IBD pulses has a counterpart within the geo-located VHF radiation sources during the displayed three milliseconds. During the 208 ms-long records in Figs. 1b and 2b, SAETTA was able to geo-locate 444 and 159 VHF sources, respectively. The number of geo-locations during all 128 events varies from 1 (our condition for including an event in the analysis) to 843 VHF sources. The first geo-located source occurred within the ±1ms window around the first detectable IBD pulse in 75 % of cases. In more than 85 % of events, the geo-located source occurring close to the first detectable magnetic-field pulse was also the most powerful one, with power varying from 8 to 36 dBW (24 dBW on average). Geo-located VHF sources occurring later in time were weaker, and, similarly as in Figs. 1b and 2b, their power did not exceed 20 dBW. VHF sources were predominantly reconstructed at an altitude between 2 and 6 km, even if some sources appeared also below and above this altitude range (for an overview, see movies S1 and S2 in Supplementary material).

Kolmasova et al. (2018) reported that individual peaks of strong VHF radiation in the raw LMA data recorded at individual stations corresponded well to the broadband pulses during lightning initiation. However, the LMA system had troubles to reconstruct geo-located VHF sources if the raw counts reached a maximum of 2000 detections within an 80-μs LMA window. In the present study, this maximum was regularly reached at the stations located close to developing discharges and continuous radiation existed in the raw data during the initial phase of IBD events. Examples of VHF radiation detected by SAETTA station B are illustrated in Figs. 1c (29 km away) and 2c (108 km away). VHF radiation in Fig.1c remained very intense up to the end of the record, while in Fig. 2c it was generally weaker and the counts and strengths of VHF sources dropped after 120 ms to very low values, suggesting a different discharge development. We inspected the evolution of strengths and counts of VHF radiation sources detected during all 128 events at all LMA stations and we found that for three quarters of them the intense VHF radiation continued to occur at least at the closest LMA station up to the end of the 208-ms long magnetic-field record, similarly to Fig. 1c. In the remaining cases, the VHF radiation substantially dropped at all LMA stations before the end of the magnetic-field record, similarly to Fig. 2c.

We illustrate the propagation of discharges starting with IBD pulses in Figs. 1d-f and 2d-f. Each dot represents one geo-located VHF source color-coded by its time of occurrence. The discharge in Fig. 1 started at an altitude of about 2 km, moved up by about two kilometers in 30 ms, and kept propagating with nearly horizontal branches in a limited interval of altitudes for 100 ms (Fig. 1b). Finally, one branch moved down back to the initiation altitude and the other one propagated horizontally. This flash was recorded during a weak lightning activity (7 flashes over 20 min). It was the first flash of a 3-flash sequence of 150-second duration with a similar vertical distribution of geo-located VHF sources. The discharge in Fig. 2 shortly propagated almost at a constant altitude (Fig. 2b). This flash was also recorded during a rather weak lightning activity (7 flashes in 12 minutes). After combining all 3D propagation maps with the information about the presence/absence of VHF sources detected at individual LMA stations for all IBD events, we identify two different propagation scenarios: the discharges continue to propagate horizontally for more than 150 ms (Type A, as in Fig. 1 – 73 %), or they fade out sooner than 150ms, typically within several tens of milliseconds (Type B, as in Fig. 2 – 27 %).

The map in Fig. 3a shows locations of the first geo-located VHF sources detected close to the first recognizable IBD pulses. Types A and B are represented by blue and red dots, respectively. Green diamonds and the turquoise star represent the locations of the SAETTA and BLESKA stations, respectively. The blue and red arrows point to the events shown in Figs. 1 and 2, respectively. Distribution of peak currents belonging to the strongest pulses which were detected by Météorage (correctly as 116 IC, misclassified as 6 CG+, 6 CG-) during all individual sequences is plotted in Fig. 3b. The median values of the peak current are 20 kA and 17 kA for types A and B, respectively. Note that these distributions are similar in both cases, and that the currents might be underestimated for both categories, as shown by Kaspar et al. (2016). The distribution of initiation heights for types A and B is again similar (Fig. 3c), with median values of 3.5 km and 3.8 km, respectively.

5. Model of isolated breakdown process

To improve our understanding of the role of LPCR in the IBD process (Nag and Rakov, 2008; Iudin et al., 2017) we investigate how the magnitude, thickness, and position of the LPCR can change the vertical electric potential. In our model, we used a charge distribution typical for an updraft thundercloud region (Stolzenburg and Marshall, 2008). It consists of a main negative layer, a main positive layer, an upper screening negative layer, and a LPCR. Our estimates of charge amounts in individual uniformly charged layers were based on measurements collected by Rakov and Uman (2003). Fig. 4a shows the charge structure together with an ambient electric field (dashed line) and electric potential (dotted line) calculated along the vertical axis of the cylindrical charge regions as a solution of the Poisson's equation in cylindrical coordinates using a successive over-relaxation method (Press et al., 1996). The domain of solution extends 20 km vertically and 20 km radially discretized on a 2D grid with a space resolution of 5 m. We fix the potential to 400 kV at an upper boundary of 20 km as Mazur and Ruhnke (1998), and to zero at the remaining boundaries. We fix this thundercloud structure and change only the parameters of the LPCR.

The LPCR default parameters in our model are as follows: a total charge of 20 C; the lower and upper boundary at 2.7 km and 3.5 km, respectively. By changing only the total charge of the LPCR stepwise from 10 C to 27.5 C, a potential well is found for charge values higher than 17.5 C (Fig. 4b). A change of the LPCR thickness from 500 m to 1000 m assuming a constant charge density of 0.9 nC/m^3 induces a potential well for LPCR thicker than 700 m (Fig. 4c). Finally, altitude shifts of the LPCR from its original altitude of 2.7 km down to 2.5 km and then 2.3 km, leads to a deepening of the potential well (Fig. 4d). The same calculations for the electric field are shown in Fig. 1S (supplementary material).

Mansell et al. (2002) predicted the existence of a critical electric field as a threshold for lightning leader propagation. Bazelyan and Raizer (2000) assume that the leader stops when the difference between the potential of the leader tip and the ambient potential is lower than about 300-400 kV. We consider only propagation of the lightning leader along the vertical axis of our model, assuming a flash initiation between the main negative charge layer and the LPCR. A lightning flash can then encounter a large potential well while propagating toward the ground as we demonstrate in Figs. 4b-4d. As a result, the leader either can stop propagating completely or can change its direction and propagates horizontally in the LPCR.

6. Discussion and summary

We have analyzed 128 sequences of IBD pulses observed simultaneously by a broadband receiver, a LMA network, and Météorage in West Mediterranean in 2015 and 2018. We verified findings of Kolmasova et al. (2018) that intense VHF radiation in raw LMA data starts with the first IBD pulse in the broadband magnetic-field measurements and that the most intense VHF radiation are often correlated with the broadband pulses. The number of VHF sources geo-located by SAETTA within the 208 ms-long magnetic-field records, varied from units to hundreds. There were only a few geo-located sources occurring simultaneously with the magnetic-field IBD pulse trains. In the majority of cases (85 %), the VHF source occurring within 1 ms around the first detectable IBD pulse was also the most powerful one detected during the IBD pulse train. Their power ranged from 8 to 36 dBW (~ 6 W to 4 kW), by about two orders of magnitude weaker than VHF power accompanying Narrow Bipolar Events reported by Bandara et al. (2020), but by two orders of magnitude stronger than VHF radiation detected around the initiation event of CG or IC discharges by Marshall et al. (2019).

We have identified two scenarios of the IBD process based on the 128 sequences: the discharge continues to propagate horizontally for more than 150 ms (Type A - 73 %) or dies out quickly, usually within several tens of milliseconds (Type B - 27 %). Typical in-cloud currents, which generated the strongest IBD pulses (~ 20 kA), are similar for both types and do not differ from peak currents, which emitted the most intense PB pulses preceding negative CG discharges in Florida, US (Karunarathne et al., 2019). Typical initiation altitudes (3.5 km, similar for both types) correspond to the region between the main negative and lower positive charge centers, where negative CG discharges are initiated (Stolzenburg and Marshall, 2008).

We verified that properties of the LPCR play a crucial role in the ability of the downward propagating leader to reach the ground. Both a larger strength and/or a lower position of the LPCR can lead to the development of a positive potential well below it. Our results are consistent with outcomes of Iudin et al. (2017) even though they used different charge distributions, positions, radii, and widths of the LPCR. Our results also agree with observation of Coleman et al. (2008) who combined balloon measurements of vertical electric field and LMA detections and found that a horizontal extension of lightning channels correlated with occurrences of potential extrema.

In conclusion, we find that IBD events described in this study are similar to PB processes preceding negative CG lightning analyzed in Kolmasova et al. (2018) which were collected by the same instrumental setup and in the same location. Our results therefore indicate that IBD processes correspond to usual negative CG discharges, which failed to propagate to ground after being blocked by an excessive LPCR. The two observed propagation scenarios are likely related to the spatial distributions and strengths of charge regions in the thundercloud. More studies are needed to find geographical or seasonal variation of the IBD processes.

Acknowledgements

The work of IK and OS was supported by European Regional Development Fund-Project CRREAT (CZ.02.1.01/0.0/0.0/15_003/0000481) and by the Praemium Academiae award of the Czech Academy of Sciences. The work of PK, AK, RL and LU was supported by the GACR grant 20-09671S. The work from ED, SC and SP was supported by CNES through the SOLID project and by ANR through the ANR-16-CE04-0005 EXAEDRE project. The SAETTA network was operated with the support from CNES, HyMeX program, and Collectivité de Corse. The broadband data are available at http://bleska.ufa.cas.cz/ersa/storage/tar/. The SAETTA data are available at http://babeta.ufa.cas.cz/repository/data_2020GL090593.html.

References

Bandara, S., T. Marshall, S. Karunarathne, & M. Stolzenburg (2020), Electric field change and VHF waveforms of Positive Narrow Bipolar Events in Mississippi thunderstorms, *Atmos. Res.243*, doi:org/10.1016/j.atmosres.2020.105000.

Bazelyan, E. M., & Y. P. Raizer (2000), *Lightning physics and lightning protection*. CRC Press.

Blanc, E., F. Lefeuvre, R. Roussel-Dupré, & J. Sauvaud (2007), TARANIS: A microsatellite project dedicated to the study of impulsive transfers of energy between the Earth atmosphere, the ionosphere, and the magnetosphere, *Adv. Space Res., 40(8), 1268–1275,* doi:10.1016/j.asr.2007.06.037.

Coleman, L. M., M. Stolzenburg, T. C. Marshall, & M. Stanley (2008), Horizontal lightning propagation, preliminary breakdown, and electric potential in New Mexico thunderstorms. *J. of Geophys. Res.: Atm.*, 113(D9), doi: 10.1029/2007JD009459.

Coquillat, S., Defer, E., de Guibert, P., Lambert, D., Pinty, J.-P., Pont, V., Prieur, S., Thomas, R. J., Krehbiel, P. R., and Rison, W.: SAETTA: high-resolution 3-D mapping of the total lightning activity in the Mediterranean Basin over Corsica, with a focus on a mesoscale convective system event, Atmos. Meas. Tech., 12, 5765–5790, https://doi.org/10.5194/amt-12-5765-2019, 2019.

Iudin, D. I., V. A. Rakov, E. A. Mareev, F. D. Iudin, A. A. Syssoev, & S. S. Davydenko (2017), Advanced numerical model of lightning development: Application to studying the role of LPCR in determining lightning type, *J. Geophys. Res. Atmos*., 122, 6416–6430, doi:10.1002/2016JD026261.

Kašpar, P., O. Santolík, I. Kolmašová, & T. Farges (2016), A model of preliminary breakdown pulse peak currents and their relation to the observed electric field pulses, *Geophys. Res. Lett*., 43, doi:10.1002/2016GL071483.

Kolmašová, I., O. Santolík, T. Farges, W. Rison, R. Lán, & L. Uhlíř (2014), Properties of the unusually short pulse sequences occurring prior to the first strokes of negative cloud-to-ground lightning flashes, *Geophys. Res. Lett., 41,* 5316–5324, doi:10.1002/2014GL060913.

Kolmašová, I., O. Santolík, T. Farges, S. A. Cummer, R. Lán, and L. Uhlíř (2016), Subionospheric propagation and peak currents of preliminary breakdown pulses before negative cloud-to-ground lightning discharges, *Geophys. Res. Lett*., 43, 1382–1391, doi:10.1002/2015GL067364.

Kolmašová, I., O. Santolík, E. Defer, W. Rison, S. Coquillat, S. Pedeboy, et al. (2018), Lightning initiation: Strong VHF radiation sources accompanying preliminary breakdown pulses during lightning initiation, *Scientific Reports,* volume 8, Article number: 3650, doi:10.1038/s41598-018-21972-z.

Kotovsky, D. A., R. C. Moore, Y. Zhu, M. D. Tran, V. A. Rakov, J. T. Pilkey, et al. (2016), Initial breakdown and fast leaders in lightning discharges producing long-lasting disturbances of the lower ionosphere, *J. Geophys.Res. Space Physics*, 121, 5794–5804, doi:10.1002/2015JA022266.

Mansell, E. R., D. R. MacGorman, C. L. Ziegler, & J. M. Straka (2002), Simulated three-dimensional branched lightning in a numerical thunderstorm model, *J. Geophys. Res. Atmos*., 107(D9), doi: 10.1029/2000JD000244.

Marshall, T., W. Schulz, N. Karunarathna, S. Karunarathne, M. Stolzenburg, C. Vergeiner, & T. Warner (2014a), On the percentage of lightning flashes that begin with initial breakdown pulses, *J. Geophys. Res. Atmos.,* 119, 445–460, doi:10.1002/2013JD020854.

Marshall, T., M. Stolzenburg, N. Karunarathna, & S. Karunarathne (2014b), Electromagnetic activity before initial breakdown pulses of lightning, *J. Geophys. Res. Atmos.*, 119, 12,558–12,574, doi:10.1002/2014JD022155.

Marshall, T., S. Bandara, N. Karunarathne, S. Karunarathne, I. Kolmasova, R. Siedlecki, & M. Stolzenburg (2019), A study of lightning flash initiation prior to the first initial breakdown pulse, *Atmospheric Research* 217,10-23, doi:10.1016/j.atmosres.2018.10.013.

Mazur, V. & L. H. Ruhnke (1998), Model of electric charges in thunderstorms and associated lightning. *J. Geophys. Res. Atmos.*, 103(D18), 23299-23308, doi:0.1029/98JD02120.

Nag, A. & V. A. Rakov (2008), Pulse trains that are characteristic of preliminary breakdown in cloud-to-ground lightning but are not followed by return stroke pulses, *J. Geophys. Res. 113*, D01102.

Nag, A., B. A. DeCarlo, & V. A. Rakov (2009), Analysis of microsecond- and submicrosecond-scale electric field pulses produced by cloud and ground lightning discharges, *Atmospheric Research 91*, 316–325, doi:10.1016/j.atmosres.2008.01.014.

Pedeboy, S. & M. Toullec (2016), Impact study of the ‘Millau Bridge’ on the local lightning occurrence. in *International Lightning Protection Symposium 2016.*

Press, W. H., S. A. Teukolsky, W. T. Vetterling, & B. P. Flannery (1996), *Numerical recipes in C*, volume 2. Citeseer.

Rakov, V. A., & M. A. Uman (2003), Lightning – Physics and effects, *Cambridge University Press*, ISBN:9780521583275.

Rhodes, C. T., X. M. Shao, P. R. Krehbiel, R. J. Thomas, & C. O. Hayeng (1994), Observations of lightning phenomena using radio interferometry, *J. Geophys. Res.*, 99, D6.

Riousset, J. A., V. P. Pasko, P. R. Krehbiel, R. J. Thomas, & W. Rison (2007), Three-dimensional fractal modeling of intracloud lightning discharge in a New Mexico thunderstorm and comparison with lightning mapping observations. *J. Geophys. Res. Atmos.*, 112(D15), doi: 10.1029/2006JD007621.

Rison, W., R.J. Thomas, P.R. Krehbiel, T. Hamlin, & J. Harlin (1999), A GPS-based Three-Dimensional Lightning Mapping System: Initial Observations in Central New Mexico, *Geophys. Res. Lett.*, 26, No. 23, 3573-3576.

Smith, E. M., Marshall, T. C., Karunarathne, S., Siedlecki, R., & Stolzenburg, M. (2018). Initial breakdown pulse parameters in intracloud and cloud-to-ground lightning flashes. J. *Geophys. Res.*Atmos. *123*, 2129–2140, doi:10.1002/2017JD027729.

Schulz, W., G. Diendorfer, S. Pedeboy, & D. Roel Poelman (2016), The European lightning location system EUCLID - Part 1: Performance analysis and validation. *Nat. Hazards Earth Syst. Sci.* **16,** 595–605.

Sharma, S.R., V. Cooray, & M. Fernando (2008), Isolated breakdown activity in Swedish lightning, *J. Atmos. Sol.-Terr. Phys. 70*, 1213– 1221, doi:10.1016/j.jastp.2008.03.003.

Stolzenburg, M. & T. C. Marshall (2008), Charge structure and dynamics in thunderstorms. *Space Science Reviews*, 137, 355-372, doi:10.1007/s11214-008-9338-z.

Tan, Y., S. Tao, & B. Zhu (2006), Fine-resolution simulation of the channel structures and propagation features of intracloud lightning. *Geophys. Res. Lett*, 33(9), doi:10.1029/2005GL025523.

Tan, Y., S. Tao, Z. Liang, and B. Zhu (2014), Numerical study on relationship between lightning types and distribution of space charge and electric potential, *J. Geophys. Res. Atmos.*, 109, 1003–1014, doi:10.1002/2013JD019983.

Thomas, R. J., P. R. Krehbiel, W. Rison, S. J. Hunyady, W. P. Winn, T. Hamlin, & J. Harlin (2004), Accuracy of the Lightning Mapping Array, *J. Geophys. Res.*, 109, D14207, doi:10.1029/2004JD004549.

Fig. 1

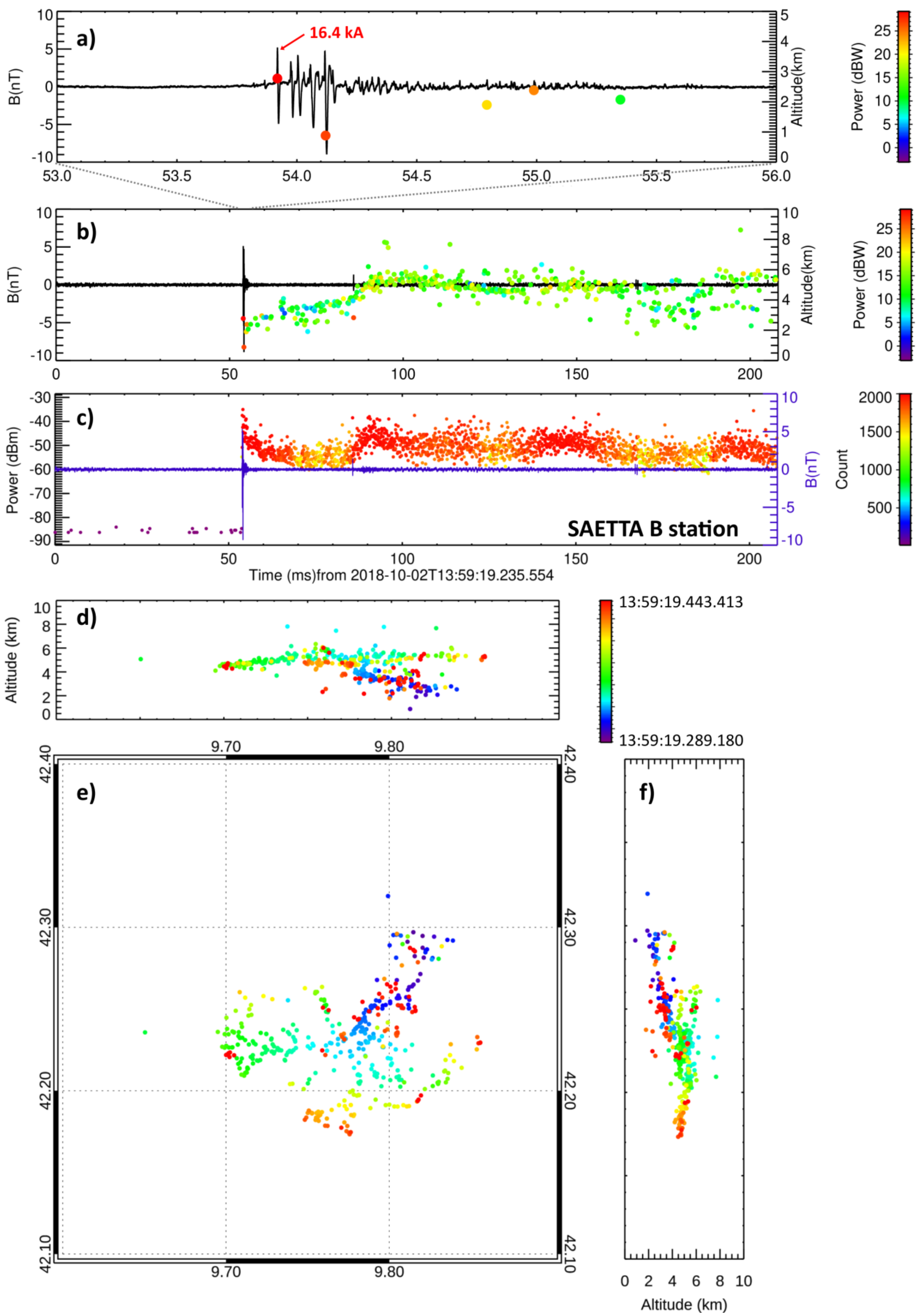

a)
16.4 kA
B(nT)
Altitude(km)
Power (dBW)
b)
B(nT)
Altitude(km)
Power (dBW)
c)
Power (dBm)
B(nT)
Count
SAETTA B station
Time (ms)from 2018-10-02T13:59:19.235.554
d)
Altitude (km)
13:59:19.443.413
13:59:19.289.180
e)
f)
Altitude (km)

Fig.1 Example of an IBD event (type A) occurring on 2 Oct 2018 at 13:55:19.236 UT: (a) 3-ms long detail of the BLESKA waveform showing a sequence of IBD pulses overlaid on altitude of geo-located SAETTA VHF radiation sources color-coded by their power; (b) the whole 208 ms-long BLESKA record with geo-located VHF radiation sources; (c) the BLESKA record with peaks of radiated VHF power recorded at the SAETTA station B (color-coded by their counts within individual 80μs LMA windows); (d–f) 3D location of VHF radiation sources color-coded by time (7 SAETTA stations minimum, $\chi^2 < 1$).

Fig. 2 Same as Fig. 1 but for an IBD event (type B) occurring on 13 Oct 2015 at 22:09:30.073 UT.

Fig. 2

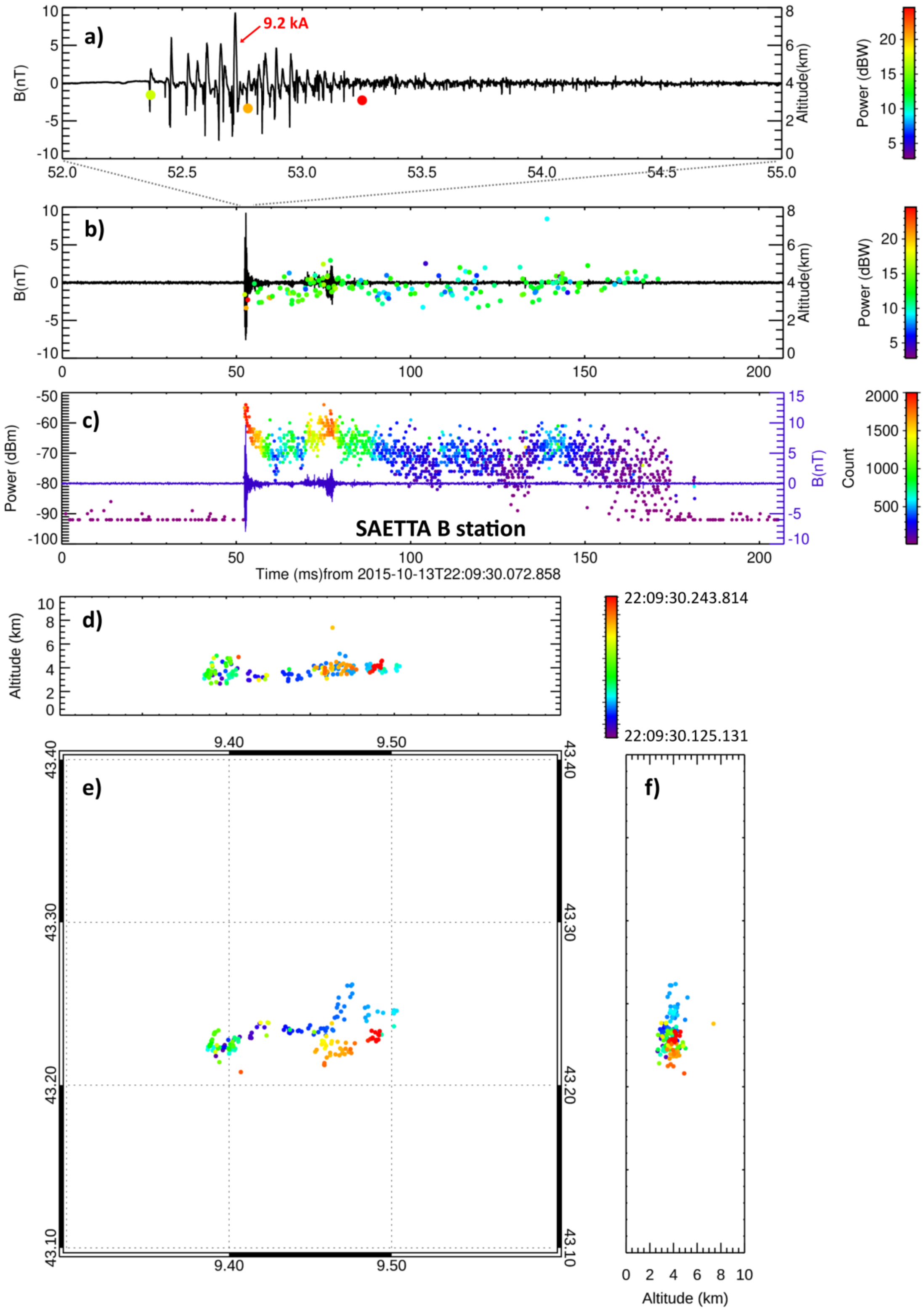
a)
9.2 kA
B(nT)
Altitude(km)
Power (dBW)
b)
c)
Power (dBm)
B(nT)
Count
SAETTA B station
Time (ms)from 2015-10-13T22:09:30.072.858
d)
Altitude (km)
22:09:30.243.814
22:09:30.125.131
e)
f)
Altitude (km)

Fig. 3

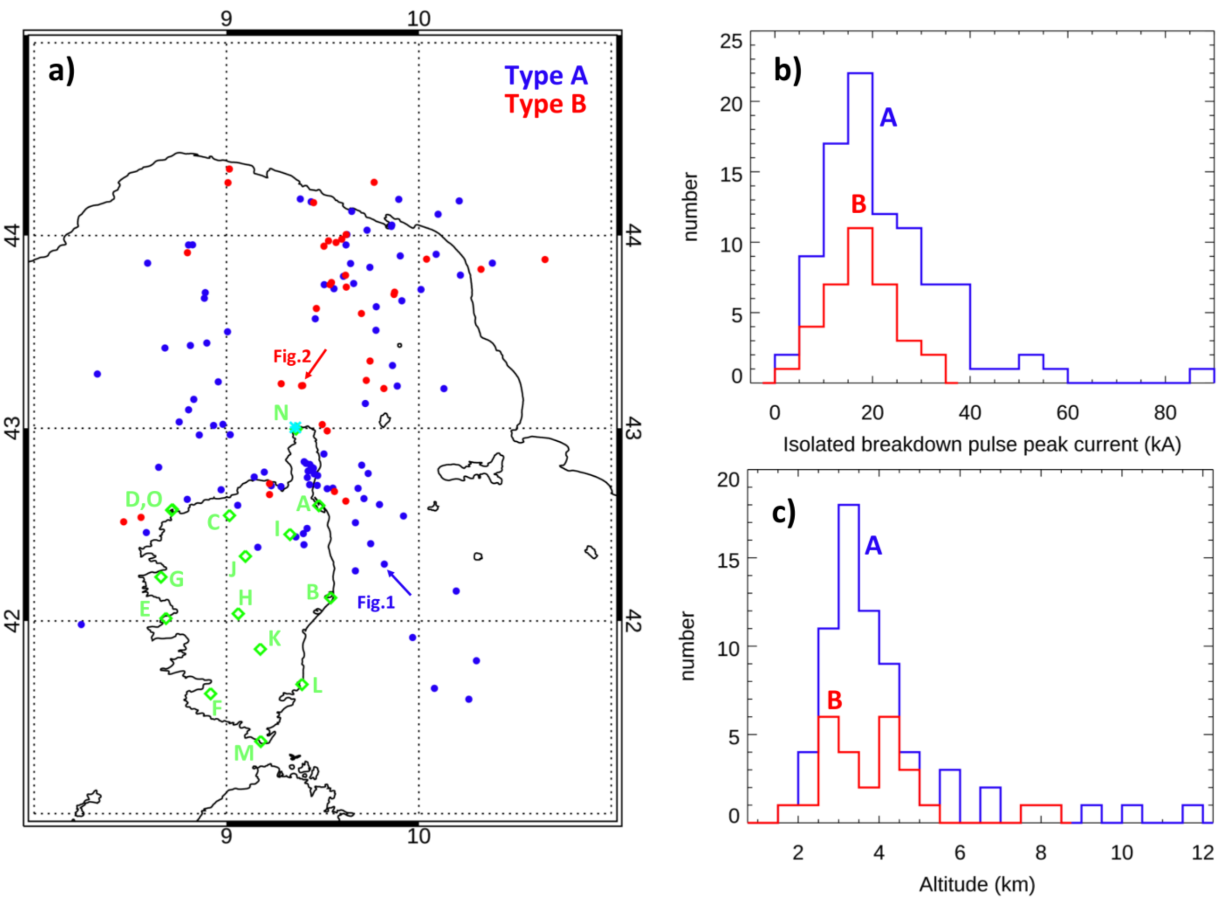

Fig.3 (a) Map showing the 2D location of the geo-located VHF sources occurring within 1ms from the first recognizable magnetic-field pulse (blue: type A, red: type B). Green diamonds show the locations of SAETTA stations. The light blue star locates the BLESKA receiver. (b) Histograms of the Météorage peak current corresponding to largest pulses identified within magnetic-field pulse sequences; (c) Histograms of initiation heights obtained as altitudes of the LMA geo-located sources occurring within 1ms from the first recognizable IBD pulse (altitude uncertainty: ~20 m above Corsica and up ~500 m at 200 km from the coast).

Fig. 4

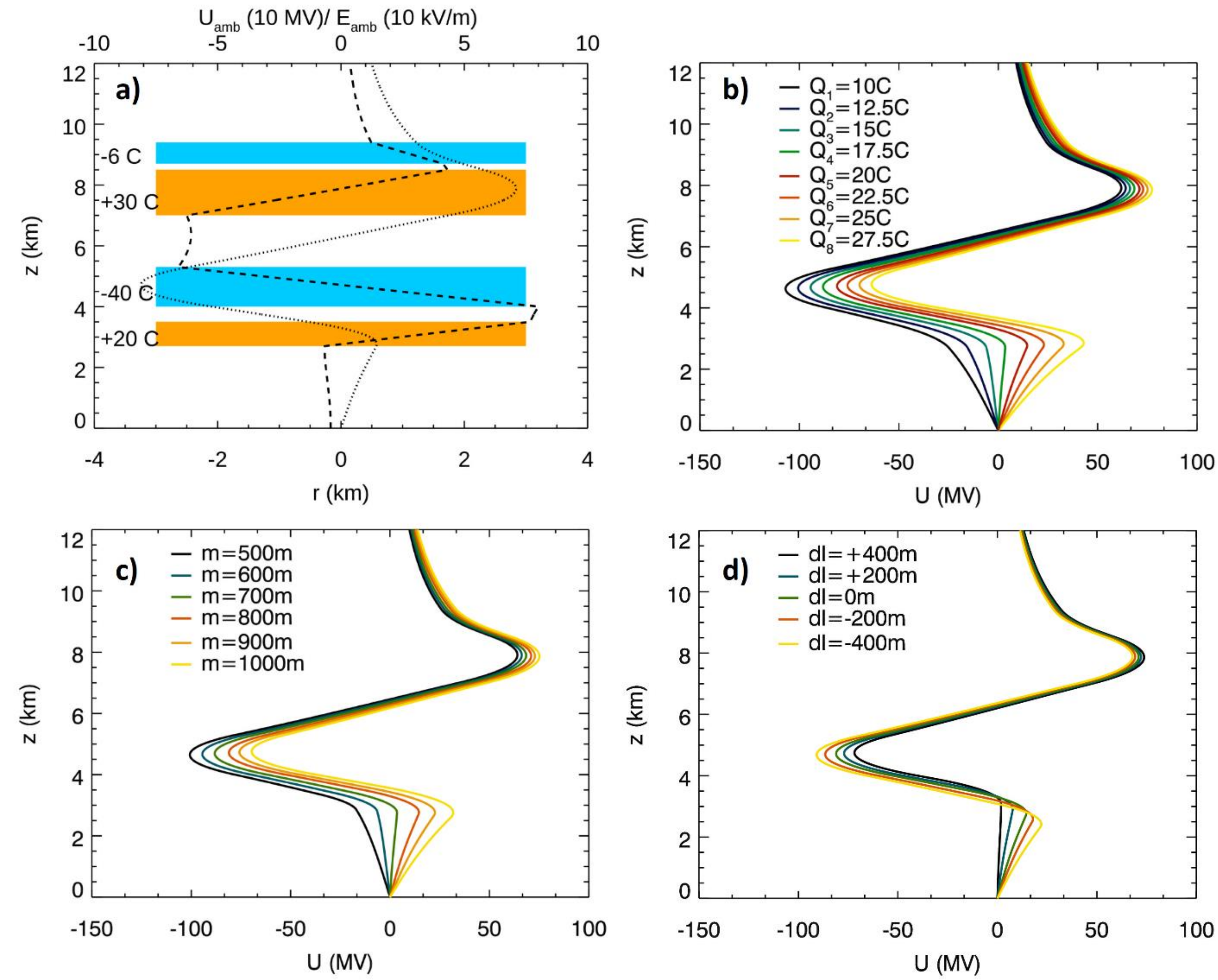

Fig.4: (a) Modeled thundercloud charge structure together with an ambient electric potential (dotted line) and an ambient electric field (dashed line), respectively. Variations of electric potential as a function of the LPCR strength (b), of the LPCR thickness (c), and of its deviation from its basic position located at 2.7 km (d).